Rotating Hele-Shaw cell with a time-dependent angular velocity

Pedro H. A. Anjos, Victor M. M. Alvarez, Eduardo O. Dias,* and José A. Miranda†
Departamento de Física, Universidade Federal de Pernambuco, Recife, Pernambuco 50670-901, Brazil
(Received 25 July 2017; published 19 December 2017)

Despite the large number of existing studies of viscous flows in rotating Hele-Shaw cells, most investigations analyze rotational motion with a constant angular velocity, under vanishing Reynolds number conditions in which inertial effects can be neglected. In this work, we examine the linear and weakly nonlinear dynamics of the interface between two immiscible fluids in a rotating Hele-Shaw cell, considering the action of a time-dependent angular velocity, and taking into account the contribution of inertia. By using a generalized Darcy's law, we derive a second-order mode-coupling equation which describes the time evolution of the interfacial perturbation amplitudes. For arbitrary values of viscosity and density ratios, and for a range of values of a rotational Reynolds number, we investigate how the time-dependent angular velocity and inertia affect the important finger competition events that traditionally arise in rotating Hele-Shaw flows.

DOI: 10.1103/PhysRevFluids.2.124003

I. INTRODUCTION

The rotating Hele-Shaw cell arrangement is a variant of the traditional viscous fingering, Saffman-Taylor instability problem [1]. In its radial geometry setup [2], the Saffman-Taylor instability occurs when a fluid is injected through a central inlet, displacing a higher viscosity fluid radially outwards in a motionless Hele-Shaw cell. This cell is an effectively two-dimensional (2D) device composed of two narrowly spaced parallel glass plates. As the initially circular fluid-fluid interface expands, it deforms, and fingerlike protuberances form. The perturbed interface evolves, and the produced fingers split at their tips, in such a way that repeated finger tip-splitting events prosper. This leads to the formation of highly branched interfacial patterns [3]. In this way, one can say that the injection-mediated, radial fingering instability is driven by the viscosity difference between the fluids, and that the most emblematic pattern formation process associated with it is finger tip splitting.

A different type of fingering instability arises if the Hele-Shaw cell is subjected to a rotational motion about an axis perpendicular to the cell plates [4]. In this alternative configuration, one has a dense inner fluid surrounded by another fluid of lower density. Under rotation, the originally circular two-fluid boundary becomes unstable and distorts due to the action of centrifugal forces [5,6]. As a result, another class of interfacial patterns emerges, being very different from the ones obtained in the injection-induced, radial fingering Saffman-Taylor situation [1–3]. Usually, the rotating fingering patterns exhibit nonsplitting fingers of different lengths that compete among themselves. So, instead of finger tip splitting, one observes the emergence of structures markedly characterized by finger length variability. Depending on the viscosity ratio between the fluids, the resulting patterns can assume a variety of shapes, ranging from relatively wide tear-drop-like structures, and thin filamented arms presenting bulbous ends, to ramified backbone morphologies. Thus, one can affirm that the centrifugal viscous fingering instability is caused by the density difference between the fluids, where the most conspicuous pattern-forming growth phenomenon is finger competition.

Over the last three decades, various aspects of the rotating Hele-Shaw cell problem have been studied both theoretically and experimentally. For example, on the experimental side, researchers have investigated the dependence of pattern morphologies on viscous [6–9] and wetting [10] effects.

*eduardodias@df.ufpe.br
†jme@df.ufpe.br

On the purely theoretical side, people have been giving continued attention to the development of rigorous exact solutions of the problem [11–15]. Investigators have also employed perturbative methods, like linear analysis [4,6,9], and weakly nonlinear mode-coupling theory [16], to better understand interface stability issues, as well as the finger competition mechanism. On the other hand, intensive numerical simulations, using several methods, including spectral [17,18], boundary-integral [19], phase-field [20], and diffuse-interface approaches [21], have also been utilized to get physical insight into finger competition and pinch-off phenomena occurring in both miscible and immiscible displacements in rotating Hele-Shaw cells. Furthermore, some research groups have looked into the role played by Coriolis forces on the interfacial dynamics in rotating Hele-Shaw flows [4,22–27].

Irrespective of the scientific validity and the significant number of investigations on the rotating Hele-Shaw cell problem (see Refs. [4–27], and references therein), the almost absolute majority of existing studies focuses on the situation in which the cell's angular velocity is constant in time. However, as pointed out in Ref. [7], in real laboratory experiments, the rotating Hele-Shaw cell cannot reach a constant angular velocity instantaneously. In reality, there is a transient interval at the beginning of each experimental run where the angular velocity rises from zero to a finite steady value. Therefore, strictly speaking, the Hele-Shaw cell angular velocity is time-dependent. Nevertheless, as also discussed in Ref. [7], under ordinary experimental conditions explored so far [zero, or nearly zero Reynolds number (Re) situation, where Re measures the ratio of inertia to viscous forces], the mentioned transient time is considerably short, in such a way that the effects of the time-varying angular velocity can be neglected.

In addition of being relevant to properly describe the unavoidable transient effects occurring even in rotating Hele-Shaw flows set to achieve a constant angular velocity [7], the effects of a legitimately time-dependent angular velocity on the fluid dynamics of such confined flows are important by themselves and only recently started to be investigated in the literature [28]. A theoretical work presented in Ref. [28] used an inviscid linear stability analysis to examine how the amplitude of the perturbed rotating two-fluid interface responds to the action of an angular velocity that varied sinusoidally with time. Their main conclusion was simply that the time-periodic angular velocity affects the threshold of the instability, tending to stabilize interfacial disturbances.

From the studies performed in Refs. [7,28], the consideration of time variation of the angular velocity is of importance to both the transient regime in usual constant angular velocity studies, as well as to linear stability investigations that consider an explicitly time-dependent angular velocity $\Omega(t)$, acting during the whole dynamic evolution of the fluid-fluid interface in rotating Hele-Shaw flows. However, it is also clear that a study of the influence of a time-dependent angular velocity on the nonlinear dynamics of ubiquitous finger competition events in rotating Hele-Shaw cells still needs to be performed. Additionally, an understanding of the physical conditions under which the role of such a time-dependent angular velocity cannot be ignored during such confined rotating flows is lacking. These are precisely the issues we intend to address in this work.

Since we focus on a situation in which two fluids flow in a rotating Hele-Shaw cell having a time-dependent angular velocity, it is natural to expect that effects connected to the acceleration of the system should be taken into account. In this framing, at least in principle, inertial effects should be instrumental in determining the pattern-forming dynamics. Therefore, in contrast to the overwhelming majority of studies carried out in the rotating Hele-Shaw cell setup, in this work we not only consider a time-dependent angular velocity, but also study its impact on the evolving two-fluid interface by taken into consideration the action of inertial effects. It should be noted that, although the assumption of negligible inertial effects (vanishing Reynolds number) is entirely reasonable and justified for most of the studies in both motionless, and rotating Hele-Shaw cells, a growing number of studies [29–35] have demonstrated it could be otherwise. In fact, for the simpler case of a single fluid displacement in a rotating Hele-Shaw cell with constant angular velocity [34], a theoretical study has shown that in the circumstances in which the fluid has low viscosity, or large density, or yet if the cell gap width, or the angular velocity are large, inertial effects can be sizable and cannot be disregarded.

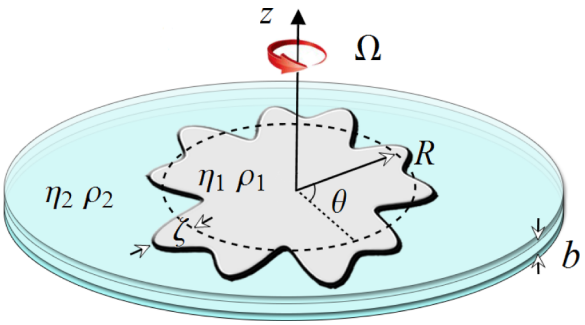

FIG. 1. Illustrative sketch of a rotating Hele-Shaw cell.

The remainder of this paper is structured as follows. Section II presents the basic setup of the physical problem and introduces the governing equations. Then, by taking inertial effects into account, and by using a generalized gap-averaged nonlinear Darcy's law, we derive a second-order mode-coupling equation that describes the time evolution of the interfacial perturbation amplitudes for the rotating Hele-Shaw cell problem with a time-dependent angular velocity. This is done by considering a general two-fluid situation, i.e., for arbitrary values of viscosity and density ratios, as well as for a range of magnitudes for the rotational Reynolds number Re. In Sec. III we discuss the impact of a time-dependent angular velocity $\Omega(t)$ and inertial effects at linear and weakly nonlinear stages of the flow. We concentrate our attention on trying to comprehend how the intrinsically nonlinear finger competition phenomenon is influenced by $\Omega(t)$ and Re. Our final conclusions are presented in Sec. IV.

II. GOVERNING EQUATIONS

A schematic representation of the rotating Hele-Shaw cell arrangement is illustrated in Fig. 1. Consider two immiscible viscous fluids in a Hele-Shaw cell of gap width b that rotates with angular velocity Ω around the z axis, which is perpendicular to the cell plates. In contrast to most theoretical works on rotating Hele-Shaw flows, we consider that the angular velocity $\Omega = \Omega(t)$ of the rotating cell can change with time. We define the rotating coordinate system in such a way that its origin is located at the center of the cell. The viscosities of the inner and outer fluids are denoted by η_1 and η_2, respectively, and the surface tension between them is σ. Likewise, the densities of the fluids are defined as ρ_1 and ρ_2.

We describe the perturbed two-fluid interface as $\mathcal{R}(\theta,t) = R + \zeta(\theta,t)$, where R is the radius of the initially circular unperturbed interface, and $\zeta(\theta,t) = \sum_{n=-\infty}^{+\infty} \zeta_n(t) \exp(in\theta)$ represents the net interface perturbation with Fourier amplitudes $\zeta_n(t)$ and discrete azimuthal wave numbers n. The perturbative weakly nonlinear model we employ keeps up to second-order terms in ζ and describes the linear and initial nonlinear dynamics of the system.

We extend the theoretical approach originally developed in Refs. [29–33] for motionless Hele-Shaw cells and expand it to rotating flows, examining a situation in which the effects of the time-dependent angular velocity of the cell plates and fluid inertia are taken into account. Within this context, as opposed to the usual Darcy's law description [3], we consider that the fluid flow in the rotating frame of reference is governed by a gap-averaged, generalized Darcy's law equation [4,6,29–35]

$$\rho_j \left[\frac{\partial \mathbf{u}_j}{\partial t} + \frac{6}{5}(\mathbf{u}_j \cdot \nabla)\mathbf{u}_j \right] = -\nabla p_j - \frac{12\eta_j}{b^2}\mathbf{u}_j - \rho_j \mathbf{\Omega} \times (\mathbf{\Omega} \times \mathbf{r}) - \rho_j \frac{d\mathbf{\Omega}}{dt} \times \mathbf{r}, \tag{1}$$

and a 2D continuity equation for incompressible fluids,

$$\nabla \cdot \mathbf{u}_j = 0. \tag{2}$$

For a detailed derivation of Eq. (1) when $\Omega = 0$, we refer the interested reader to an Appendix presented in Ref. [29]. An alternative derivation is given in Ref. [30]. For the introduction of the rotational terms see, for instance, Refs. [22,23]. In Eqs. (1) and (2), $\mathbf{u}_j = \mathbf{u}_j(r,\theta)$ and $p_j = p_j(r,\theta)$ denote, respectively, the gap-averaged velocity and pressure for fluids $j = 1$ (inner fluid), and $j = 2$ (outer fluid). The time-dependent angular velocity $\mathbf{\Omega} = \Omega(t)\hat{\mathbf{z}}$, where $\hat{\mathbf{z}}$ is the unit vector in the z direction, and $\mathbf{r}$ is the position vector (in the cell plane) of a fluid element measured from the rotation axis. The two last terms on the right-hand side of Eq. (1) represent, respectively, the centrifugal and the angular acceleration contributions. Here we focus on understanding the action of the time-dependent angular velocity and fluid inertia on the interface dynamics, and neglect gravity and Coriolis effects.

Rescaling lengths by $L = R$, and velocities by a characteristic velocity $U = (\rho_1 {\Omega_0}^2 b^2 R)/(12\eta_1)$, the generalized Darcy's law (1) can be conveniently rewritten in a *dimensionless* form as

$$\mathrm{Re}^2\alpha_j\left[\frac{\partial \mathbf{u}_j}{\partial t} + \frac{6}{5}(\mathbf{u}_j\cdot\nabla)\mathbf{u}_j\right] = -\nabla p_j - \beta_j\mathbf{u}_j + \mathrm{Re}^2\alpha_j[\Omega^2 r\hat{\mathbf{r}} - \dot{\Omega}r\hat{\boldsymbol{\theta}}], \tag{3}$$

where $\beta_j = \eta_j/\eta_1$, $\alpha_j = \rho_j/\rho_1$, and $\hat{\theta}$ ($\hat{\mathbf{r}}$) is the unit vector in the azimuthal (radial) direction. The overdot denotes total time derivative, so that $\dot{\Omega} = d\Omega/dt$. In Eq. (3) the Reynolds number Re quantifies the effect of fluid inertia on the rotating flow and is defined as

$$\mathrm{Re} = \frac{\rho_1\Omega_0 b^2}{12\eta_1}, \tag{4}$$

where Ω_0 is a characteristic angular velocity [see Eq. (28)]. From this point on, we work with the dimensionless version of the equations.

At this point, we discuss an important issue regarding the usual Darcy's law [1,3], and its generalized version [Eq. (3)]. In most works dealing with rotating Hele-Shaw flows [5–21], where the cell rotates with constant angular velocity and inertial effects are neglected (i.e., $\mathrm{Re} = 0$), the governing equation of the system is the usual Darcy's law [1,3], where the fluid velocity is simply proportional to the gradient of the pressure. In this situation, it is possible to relate the fluid velocity to a scalar velocity potential due to the irrotational nature of the flow. However, when both a time-varying angular velocity and inertial effects [for which $\mathrm{Re} \neq 0$] are taken into account, as considered in the present work, the situation is far more complex. Under such more complicated circumstances, the flow is described by the generalized Darcy's law (3), which exhibits a nonzero rotational nature, as one can readily verify by taking the curl operator on both sides of Eq. (3). Hence, we cannot write the velocity field as a gradient of a scalar velocity potential. Considering the nonpotential nature of the flow, and in agreement with the extensive literature in rotating Hele-Shaw flows [4–27], we analyze a low (but nonvanishing) Reynolds number situation. Under this condition, and by noticing the dependence of Eq. (3) on Re^2, we asymptotically expand the velocity, as well as the pressure field at lowest nonzero order in Re^2 as

$$\mathbf{u}_j \simeq \mathbf{u}_j^{(0)} + \mathrm{Re}^2\mathbf{u}_j^{(1)}, \tag{5}$$

$$p_j \simeq p_j^{(0)} + \mathrm{Re}^2 p_j^{(1)}, \tag{6}$$

where $\mathrm{Re}^2 \ll 1$, $\mathbf{u}_j^{(0)}$ ($p_j^{(0)}$) is the zeroth-order viscous term, and $\mathbf{u}_j^{(1)}$ ($p_j^{(1)}$) the first-order inertial contribution for the velocity (pressure) field. It should be stressed that our perturbative approach performs two types of independent expansions: while the dynamic quantities (velocity and pressure) are expanded up until first order in Re^2 [Eqs. (5) and (6)], the interface itself is expanded up to second order in ζ. The asymptotic expansions we do for the velocity and pressure in terms of Re^2 are performed at the level of the generalized Darcy's law [Eq. (3)], prior to the expansion in ζ. Then the various velocity and pressure terms (already decomposed in terms of Re^2) are expanded in terms of ζ, when they are taken at the fluid-fluid interface $r = \mathcal{R}$.

By substituting Eqs. (5) and (6) into Eq. (3), and only keeping zero order terms in Re^2, we promptly verify that

$$\beta_j \mathbf{u}_j^{(0)} = -\nabla p_j^{(0)}, \tag{7}$$

which is exactly the usual Darcy's law [1,3], valid for the vanishing Re case. By the reasons discussed in the previous paragraph, the flow is irrotational for the zeroth-order velocity ($\nabla \times \mathbf{u}_j^{(0)} = 0$), and applying the incompressibility condition for $\mathbf{u}_j^{(0)}$ ($\nabla \cdot \mathbf{u}_j^{(0)} = 0$), we can define a zeroth-order velocity potential $\mathbf{u}_j^{(0)} \equiv -\nabla \phi_j^{(0)}$. Actually, one can easily see that the zeroth-order velocity potential $\phi_j^{(0)}$ obeys Laplace's equation $\nabla^2 \phi_j^{(0)} = 0$. Under these circumstances, the solution for $\phi_j^{(0)}$ in terms of the perturbation amplitudes ζ_n is the same as that for the rotating Hele-Shaw cell problem when both inertia and the time dependence of the angular velocity are not taken into account [5,6,16].

We now proceed to obtain the first-order velocity contribution $\mathbf{u}_j^{(1)}$ in terms of ζ_n. To do it, we substitute Eq. (5) and Eq. (6) into Eq. (3), and keep terms up to order Re^2, to obtain

$$\mathrm{Re}^2 \alpha_j \nabla \left[\frac{\partial \phi_j^{(0)}}{\partial t} - \frac{3}{5} \left| \nabla \phi_j^{(0)} \right|^2 \right] = \nabla p_j^{(0)} + \mathrm{Re}^2 \nabla p_j^{(1)} + \beta_j \left(-\nabla \phi_j^{(0)} + \mathrm{Re}^2 \mathbf{u}_j^{(1)} \right) - \mathrm{Re}^2 \alpha_j [\Omega^2 r \hat{\mathbf{r}} - \dot{\Omega} r \hat{\boldsymbol{\theta}}]. \tag{8}$$

By applying the curl on both sides of Eq. (8), we obtain a much simpler expression

$$\beta_j \nabla \times \mathbf{u}_j^{(1)} = -\alpha_j \dot{\Omega} \nabla \times (r \hat{\boldsymbol{\theta}}). \tag{9}$$

However, by inspecting Eq. (9), we realize that $\mathbf{u}_j^{(1)}$ can be expressed as

$$\beta_j \mathbf{u}_j^{(1)} = -\alpha_j \dot{\Omega} r \hat{\boldsymbol{\theta}} - \nabla \phi_j^{(1)}, \tag{10}$$

where $\phi_j^{(1)} = \phi_j^{(1)}(r, \theta)$ is a scalar function to be determined. From Eq. (10) it is apparent that $\mathbf{u}_j^{(1)}$ cannot be written solely as a gradient of a scalar function, immediately characterizing its nonpotential nature.

In order to obtain $\phi_j^{(1)}$, we take the divergence of Eq. (10):

$$\nabla \cdot \mathbf{u}_j^{(1)} = -\frac{\nabla^2 \phi_j^{(1)}}{\beta_j}. \tag{11}$$

On the other hand, we see that by taking into consideration the continuity equation (2), and using the fact that $\nabla \cdot \mathbf{u}_j^{(0)} = 0$, Eq. (5) implies that $\nabla \cdot \mathbf{u}_j^{(1)} = 0$. In this way, by utilizing Eq. (11), one can verify that $\phi_j^{(1)}$ satisfies Laplace's equation ($\nabla^2 \phi_j^{(1)} = 0$). Thus, the general solution for $\phi_j^{(1)}$ can be written as

$$\phi_j^{(1)} = \sum_{n \neq 0} \phi_{jn}^{(1)}(t) r^{-1^{(j+1)}|n|} \exp(in\theta). \tag{12}$$

To determine the coefficients $\phi_{jn}^{(1)}(t)$ that appear in Eq. (12) up to second order in the perturbation amplitudes ζ_n, we use the kinematic boundary condition [3,6]

$$\frac{\partial \mathcal{R}}{\partial t} = (\mathbf{u}_j \cdot \hat{\mathbf{r}})_{r=\mathcal{R}} - \left[\frac{1}{r} \frac{\partial \mathcal{R}}{\partial \theta} (\mathbf{u}_j \cdot \hat{\theta}) \right]_{r=\mathcal{R}}, \tag{13}$$

which states that the normal components of each fluid velocity are continuous at the interface. By doing this, we obtain

$$\phi_{jn}^{(1)} = (-1)^{j+1} i \alpha_j \mathrm{sgn}(n) \dot{\Omega} \zeta_n - i \alpha_j \dot{\Omega} \sum_{n' \neq 0} n' \left[\mathrm{sgn}(nn') + \frac{(-1)^j}{|n|} \right] \zeta_{n'} \zeta_{n-n'}. \tag{14}$$

Substituting the resulting expression for $\phi_j^{(1)}$ into Eq. (10), we have the velocity field $\mathbf{u}_j^{(1)}$ completely determined in terms of the perturbation amplitudes ζ_n.

Since we now have determined the velocity field $\mathbf{u}_j$, we are able to calculate the zeroth, and the first-order contributions for the pressure field p_j. To obtain the zeroth-order pressure, we substitute $\mathbf{u}_j^{(0)} = -\nabla\phi_j^{(0)}$ into Eq. (7), and integrate. After dropping an arbitrary constant of integration, $p_j^{(0)}$ is written as

$$p_j^{(0)} = \beta_j \phi_j^{(0)}. \tag{15}$$

Notice that here (i.e., for $\mathrm{Re} = 0$), the velocity potential $\phi_j^{(0)}$ and the pressure $p_j^{(0)}$ stand for almost identical quantities, differing only by β_j.

As for the first-order pressure, we go on as follows. We substitute Eq. (10) into Eq. (8), collect together only the terms of order Re^2, and integrate, to obtain

$$p_j^{(1)} = \alpha_j \left[\frac{\partial \phi_j^{(0)}}{\partial t} - \frac{3}{5} \left| \nabla \phi_j^{(0)} \right|^2 \right] + \alpha_j \Omega^2 \frac{r^2}{2} + \phi_j^{(1)}. \tag{16}$$

In order to fully specify the free boundary, interfacial problem, we still need to consider an additional boundary condition. This remaining boundary condition, known as the Young-Laplace equation [3,6], connects the pressure jump (or, the jump in the normal stress) across the two-fluid interface, with the surface tension, and the principal interface curvatures

$$(p_1 - p_2)_{r=\mathcal{R}} = B \left[\kappa + \frac{8}{\pi} q \right]_{r=\mathcal{R}}, \tag{17}$$

where

$$B = \frac{\pi \sigma}{4 \rho_1 {\Omega_0}^2 R^3} \tag{18}$$

represents a rotational Bond number that measures the ratio of surface tension to centrifugal forces, and $q = R/b$ is the aspect ratio. The first term on the right-hand side of Eq. (17) expresses the contribution related to surface tension σ, and the interfacial curvature κ in the plane of the Hele-Shaw cell. The factor $\pi/4$ that appears in the Bond number (18) is purely a capillary static effect, coming from the z average of the mean interfacial curvature [36]. The $\pi/4$ factor was absorbed in the Bond number, just promoting a small decrease in its magnitude in comparison to the situation in which it is neglected. Consequently, the results presented in this work do not strongly depend on this $\pi/4$ correction to the vertical curvature. The second term on the right-hand side of Eq. (17) accounts for the contribution of the constant curvature $(2/b)$ associated with the interface profile in the direction perpendicular to the Hele-Shaw cell plates. Notice that our Eq. (17) is a simplified version of more sophisticated versions of the pressure boundary condition that take into account wetting film effects [36,37]. Under certain circumstances, a thin wetting film of the driven fluid will be left adhering to the Hele-Shaw cell plates as the fluid-fluid interface moves. Variations in thickness of this film causes the curvature in the direction perpendicular to the Hele-Shaw cell plates to be velocity dependent, as proposed by Park and Homsy in Ref. [36]. The presence of such wetting film reintroduces complicated three-dimensional effects into the problem. Ignoring the action of the wetting thin film to the in-plane curvature corrections in the dynamics of the interface modes is equivalent to neglect dissipation in the films. So ignoring such a dynamic correction to the in-plane curvature could indeed be of significance for a more complete analysis of the interface dynamics. Although the inclusion of such a laborious wetting film contribution is beyond the scope of our current weakly nonlinear study for nonzero Re, we direct the predisposed reader to Refs. [38,39] for a detailed description of the action of wetting on the dynamics of injection-driven, and lifting Hele-Shaw cell flows when $\mathrm{Re} = 0$.

In the pursuit of a dynamic equation for the time evolution of ζ_n, we substitute Eqs. (15) and (16) into $p_j = p_j^{(0)} + \mathrm{Re}^2 p_j^{(1)}$ [Eq. (6)] and evaluate the resulting expression at the perturbed interface

$r = \mathcal{R}$. Then, by substituting p_1 and p_2 into the pressure boundary condition (17), we get the following dynamic equation for the system:

$$\left\{\phi_1^{(0)} - \beta\phi_2^{(0)} + \mathrm{Re}^2\left[\left(\frac{\partial\phi_1^{(0)}}{\partial t} - \frac{3}{5}\left|\nabla\phi_1^{(0)}\right|^2\right) + \Omega^2\frac{r^2}{2} + \phi_1^{(1)} - \alpha\left(\frac{\partial\phi_2^{(0)}}{\partial t} - \frac{3}{5}\left|\nabla\phi_2^{(0)}\right|^2\right)\right.\right.$$
$$\left.\left. - \alpha\Omega^2\frac{r^2}{2} - \phi_2^{(1)}\right]\right\}_{r=\mathcal{R}} = B\left[\kappa + \frac{8}{\pi}q\right]_{r=\mathcal{R}}, \tag{19}$$

where the parameters $\alpha = \rho_2/\rho_1$ and $\beta = \eta_2/\eta_1$ are the density and the viscosity ratios, respectively.

Finally, by keeping terms up to second order in ζ in Eq. (19), and Fourier transforming, we obtain the equation of motion for the perturbation amplitudes (for $n \neq 0$):

$$\mathrm{Re}^2\ddot{\zeta}_n + \left(\frac{1+\beta}{1+\alpha}\right)\dot{\zeta}_n - \left\{\Lambda(n) + \mathrm{Re}^2|n|\left[\left(\frac{1-\alpha}{1+\alpha}\right)\Omega^2 + i\,\mathrm{sgn}(n)\dot{\Omega}\right]\right\}\zeta_n$$
$$= \sum_{n'\neq 0}[\mathcal{F}(n,n') + \mathrm{Re}^2\mathcal{K}(n,n')]\zeta_{n'}\zeta_{n-n'} + \sum_{n'\neq 0}\mathcal{G}(n,n')\dot{\zeta}_{n'}\zeta_{n-n'}$$
$$+\mathrm{Re}^2\sum_{n'\neq 0}[\mathcal{L}(n,n')\ddot{\zeta}_{n'}\zeta_{n-n'} + \mathcal{H}(n,n')\dot{\zeta}_{n'}\dot{\zeta}_{n-n'}], \tag{20}$$

where

$$\Lambda(n) = |n|\left[\frac{B}{1+\alpha}(1-n^2)\right]. \tag{21}$$

The second-order mode-coupling terms are given by

$$\mathcal{F}(n,n') = -|n|\frac{B}{1+\alpha}\left[1 - \frac{n'}{2}(3n'+n)\right], \tag{22}$$

$$\mathcal{K}(n,n') = |n|\left(\frac{1-\alpha}{1+\alpha}\right)\left\{\frac{\Omega^2}{2} - in'\dot{\Omega}\left[\mathrm{sgn}(nn') - \frac{1}{|n|} - 1\right]\right\}, \tag{23}$$

$$\mathcal{G}(n,n') = \left(\frac{1-\beta}{1+\alpha}\right)\{|n|[\mathrm{sgn}(nn') - 1] - 1\}, \tag{24}$$

$$\mathcal{L}(n,n') = \left(\frac{1-\alpha}{1+\alpha}\right)\{|n|[\mathrm{sgn}(nn') - 1]\} - 1, \tag{25}$$

and

$$\mathcal{H}(n,n') = |n|\left(\frac{1-\alpha}{1+\alpha}\right)\left(\mathrm{sgn}(nn') + \frac{3}{5}\{\mathrm{sgn}[n'(n-n')] - 1\}\right) - 1, \tag{26}$$

where the sgn function equals ± 1 according to the sign of its argument.

Expressions (20)–(26) represent the mode-coupling equations of a quite general viscous fingering problem in a rotating Hele-Shaw cell, constituting one of the central results of this work. These equations open up the possibility to investigate the time evolution of the perturbation amplitudes (accurate to second order) considering the action of a time-dependent angular velocity and inertia. This is valid for arbitrary values of the viscosity (β) and density (α) ratios, and the rotational Bond number B, under low (but nonvanishing) Reynolds numbers Re ($\mathrm{Re}^2 \ll 1$). For the particular case in which $\alpha \to 0$, $\beta \to 0$ and $\dot{\Omega} = 0$, Eq. (20) reproduces the simpler results obtained in Ref. [34] for the corresponding one-fluid version of the problem with constant angular velocity.

Despite the complex functional form of Eqs. (20)–(26), as we will see in the following section, they furnish a fairly simple picture to the linear and weakly nonlinear phenomena that occur in

rotating Hele-Shaw flows. In addition to providing relevant information about the linear stage of the dynamics (Sec. III A), they offer useful insight into the response of the important finger competition events to the action of Ω and Re (Sec. III B).

III. EFFECTS OF TIME-DEPENDENT ANGULAR VELOCITY AND INERTIA

A. Linear stage

Although the main focus of our study is to examine the impact of $\Omega(t)$ and Re on the intrinsically nonlinear finger competition dynamics in rotating Hele-Shaw cells, in this section we briefly discuss some noteworthy aspects related to the linear stability of the system.

Here our leading goal is to analyze the influence of a time-dependent angular velocity and fluid inertia on the two-fluid interface at very early time stages of the flow dynamics. In this initial time regime, the fluid-fluid interface is just mildly deformed by centrifugal forces. Under these conditions, the interfacial perturbations ζ are so small that second-order and higher-order terms in ζ can be safely neglected. This is the reason why such an initial pattern formation stage is commonly referred to as the "linear" dynamical stage (meaning, linear in ζ). Within this linear framework, we can ignore the second-order terms in ζ that appear in Eq. (20), in such a way that the equation of motion for the perturbation amplitudes is significantly simplified, being reduced to

$$\mathrm{Re}^2\,\ddot{\zeta}_n + \left(\frac{1+\beta}{1+\alpha}\right)\dot{\zeta}_n - \left\{\Lambda(n) + \mathrm{Re}^2|n|\left[\left(\frac{1-\alpha}{1+\alpha}\right)\Omega^2 + i\,\mathrm{sgn}(n)\dot{\Omega}\right]\right\}\zeta_n = 0. \tag{27}$$

Note that, since the rotating Hele-Shaw cell plates accelerate, the coefficients in Eq. (27) that involve $\Omega(t)$ and $\dot{\Omega}(t)$ do depend on time. For a general functional form of $\Omega(t)$, this implies in a serious impediment to calculate a closed-form analytical expression for the linear growth rate of the system. Hence, already at the linear stage, the rotating Hele-Shaw cell problem with a general time-dependent angular velocity $\Omega(t)$ is usually not amenable to analytical treatment. Therefore, in general one defines the linear growth rate as $\lambda(n,t) = \mathrm{Real}[\dot{\zeta}_n/\zeta_n]$ and often deal with it by numerically solving Eq. (27).

Before we continue, it is worth making a few remarks about the particular time-dependent angular velocity that will be used throughout this work to illustrate our results. In principle, the functional form of $\Omega(t)$ can be quite general. However, to keep a close connection with real life experiments in rotating Hele-Shaw cells, we consider the specific functional form used in the experimental measurements carried out in Ref. [7]:

$$\Omega(t) = \Omega_0[1 - \exp(-\gamma t)], \tag{28}$$

where Ω_0 is the asymptotic, steady angular velocity, and γ is a positive constant. Notice that we can control the intensity of the plates rotation acceleration by changing the value of γ. In this way, the limit of constant angular velocity is reached by taking $\gamma \to \infty$.

Providentially, for the specific functional form given by Eq. (28), we find a closed-form solution for the differential equation (27), which reads

$$\begin{aligned}\zeta_n(t) = \exp&\left\{-[\sqrt{\delta^2+4c_1(n)}+\delta]t/2 - \frac{\sqrt{c_3(n)}}{\gamma}\exp(-\gamma t)\right\}\\ &\times\left\{A_1 U\left[\frac{\frac{c_2(n)}{\sqrt{c_3(n)}}+\gamma+\sqrt{\delta^2+4c_1(n)}}{2\gamma}, 1+\frac{\sqrt{\delta^2+4c_1(n)}}{\gamma}, \frac{2\sqrt{c_3(n)}}{\gamma}\exp(-\gamma t)\right]\right.\\ &\left.+A_2 L\left[\frac{-\frac{c_2(n)}{\sqrt{c_3(n)}}-\gamma-\sqrt{\delta^2+4c_1(n)}}{2\gamma}, \frac{\sqrt{\delta^2+4c_1(n)}}{\gamma}, \frac{2\sqrt{c_3(n)}}{\gamma}\exp(-\gamma t)\right]\right\},\end{aligned} \tag{29}$$

where U is the confluent hypergeometric function of the second kind, L is a generalized Laguerre

polynomial,

$$\delta = \frac{1}{\mathrm{Re}^2}\left(\frac{1+\beta}{1+\alpha}\right), \tag{30}$$

$$c_1(n) = \frac{1}{\mathrm{Re}^2}\Lambda(n) + |n|\left(\frac{1-\alpha}{1+\alpha}\right)\Omega_0^2, \tag{31}$$

$$c_2(n) = i\Omega_0\gamma n - 2|n|\left(\frac{1-\alpha}{1+\alpha}\right)\Omega_0^2, \tag{32}$$

and

$$c_3(n) = |n|\left(\frac{1-\alpha}{1+\alpha}\right)\Omega_0^2. \tag{33}$$

In Eq. (29) the constants A_1 and A_2 are determined by the initial conditions. In spite of the somewhat cumbersome nature of this linear closed-form solution, now the linear growth rate $\lambda(n,t) = \mathrm{Real}[\dot{\zeta}_n/\zeta_n]$ can be evaluated by directly utilizing Eq. (29).

In seeking to strengthen the pragmatic and academic relevance of our study, during the rest of this work we ensure that the values of all relevant dimensionless parameters we use are consistent with realistic physical quantities related to existing rotating Hele-Shaw cell arrangements and with material properties of the fluids [6–10]. It should be stressed that existing experimental studies in rotating Hele-Shaw cell with constant angular velocity are performed under considerably low Reynolds number conditions. In these situations, the largest Reynolds number used was $\mathrm{Re} = 0.04$ [9]. However, from the typical Hele-Shaw cell parameters (i.e., cell gap thickness, and cell angular velocity) and material properties of the fluids involved (viscosities, densities, and surface tension values), considerably larger values for genuine Reynolds numbers could be used. For instance, Reynolds numbers like $\mathrm{Re} = 0.1$ and $\mathrm{Re} = 0.3$ are perfectly achievable [5–10,29,32]. So, in our current theoretical study, in order to examine the role played by inertial effects and $\Omega(t)$, we consider Reynolds numbers varying in the perfectly feasible range $O(10^{-2}) \leqslant \mathrm{Re} \leqslant O(10^{-1})$.

Before continuing with our linear analysis, we make a few relevant observations about Eq. (28). Although our mode-coupling results given by Eqs. (20)–(26) are valid and accurate for any general functional form $\Omega(t)$ for a time-dependent angular velocity, here we justify the reason for choosing the specific exponential form given by Eq. (28) to exemplify our theoretical results. In the end, the utilization of Eq. (28) was motivated by practical reasons, in the sense that this particular functional form arises, and has already been implemented, and analyzed, in real life rotating Hele-Shaw cell experiments performed in Ref. [7]. Nonetheless, as commented in Sec. I, the angular velocity given in Eq. (28) expresses a transient regime that actually occurs during a constant angular velocity Hele-Shaw cell situation, since in practice the cell cannot reach a constant angular velocity instantaneously. The experimental verifications carried out in Ref. [7] have shown that, under the very low Reynolds number conditions of their experiments [$\mathrm{Re} \leqslant O(10^{-2})$], such a short-lived time-dependent velocity has no influence whatsoever on the fluid dynamic evolution of their rotating Hele-Shaw cell problem. So one could wonder what is the point of using this apparently uninfluential time-dependent angular velocity form in our current investigation. As it turns out, in this work, we study a time-dependent angular velocity rotating Hele-Shaw problem, by taking into consideration the role played by inertial effects, $\Omega(t)$, and the acceleration of the Hele-Shaw plates, which is quantified by γ. Therefore, during our study we are allowed to consider Reynolds number values that are larger than those considered in Ref. [7]. In addition, we can also deal with lower values of γ so that the transient regime of the rotating process can take much longer than those observed in usual rotating experiments [6–10]. This opens up the convenient possibility of testing how the time-dependent angular velocity given by Eq. (28) affects the linear and weakly nonlinear dynamics of the rotating Hele-Shaw cell problem when inertial effects are non-negligible [i.e., under the action of larger Reynolds number values, where $\mathrm{Re} \sim O(10^{-1})$] and for an arbitrary duration of the rotational acceleration regime.

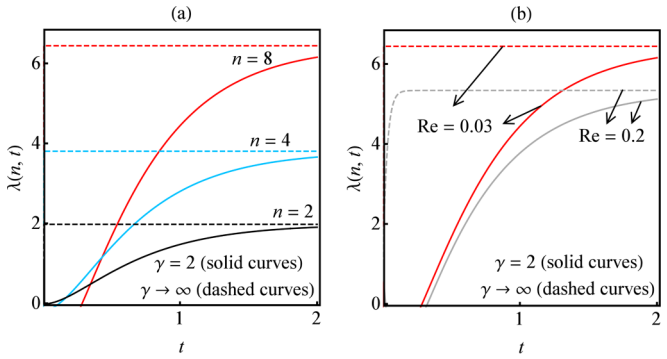

FIG. 2. Linear growth rate $\lambda(n,t)$ as a function of time t, for $\alpha = 10^{-3}$, $\beta = 0$, and $B = 3.0 \times 10^{-3}$. The action of both a constant ($\gamma \to \infty$), and a time-dependent ($\gamma = 2$) angular velocity is examined. (a) Re $= 0.03$, $n = 2$, $n = 4$, and $n = 8$. (b) $n = 8$, and two Reynolds numbers (Re $= 0.03$, and Re $= 0.2$) are considered.

Therefore, the use of Eq. (28) to illustrate our results does not mean that our study is restricted to analyzing only transient effects of a particular time-dependent angular velocity on the dynamics of the rotating flow system. After all, our Eqs. (20)–(26) are valid and accurate for any general functional form $\Omega(t)$, in the presence or absence of an eventual transient regime.

Now, to examine how the linear growth rate behaves as time advances, we analyze Fig. 2. For the sake of simplicity, we concentrate our attention on a physical situation that is commonly explored in actual rotating Hele-Shaw cell experiments [6–10], where an initial circular drop of a viscous and dense oil is surrounded by air (of negligible density and viscosity). In this case, consistently with usual experiments, the values we take for the density and viscosity ratios are $\alpha = 10^{-3}$ and $\beta = 0$, respectively. Furthermore, we consider the action of both a constant angular velocity ($\gamma \to \infty$, represented by dashed curves), as well as a time-dependent angular velocity ($\gamma = 2$, pictured by solid curves). A typical Bond number is taken as $B = 3.0 \times 10^{-3}$.

In Fig. 2(a) we plot the linear growth rate $\lambda(n,t)$ as a function of time t, for three representative Fourier modes: $n = 2$, $n = 4$, and $n = 8$. Moreover, we set a very small value for the Reynolds number, Re $= 0.03$. By inspecting Fig. 2(a), we verify that for a constant angular velocity, regardless of the Fourier mode considered, the growth rate does not depend on time. This is actually in accordance with the results previously obtained in Ref. [34]. Nonetheless, a notably distinct behavior is found when the angular velocity varies in time: if $\gamma = 2$, we observe that the growth rate evolves in time differently for each mode n, and its magnitude tends asymptotically to the corresponding constant angular velocity values at later times.

Interestingly, for $\gamma = 2$ in Fig. 2(a), we identify the existence of a series of critical times at which the two-fluid interface becomes unstable [i.e., $\lambda(n,t) > 0$] for a given mode n. It is also clear that modes having lower n become unstable earlier than larger Fourier modes. This effect occurs due to the action of the augmenting angular velocity that destabilizes the interface in such a way that higher Fourier modes become increasingly more unstable as time progresses. Of course, this is not detected if the angular velocity is constant in time. Curiously, this time-varying rotating flow behavior is quite similar to the cascade growth of the Fourier amplitudes encountered in injection-driven radial Hele-Shaw flows [40,41]. However, in contrast to the rotating system we study here [for which $\Omega = \Omega(t)$, and R is constant], in the injection-driven process, the critical times arise because the unperturbed interface radius increases with time [i.e., because $R = R(t)$].

In order to expressly probe the role played by inertial effects at the linear regime, in Fig. 2(b) we show how the growth rate evolves in time, for two values of the Reynolds number: a very small one, Re $= 0.03$, and another considerably larger, given by Re $= 0.2$. Here we describe things for a fixed Fourier mode, namely, for $n = 8$. By examining Fig. 2(b), we see that inertia tends to stabilize the two-fluid interface in two different ways: when a higher Reynolds number is considered (Re $= 0.2$),

we observe (i) a lowering of the growth rate magnitude and (ii) a small delay in the instant of time at which the Fourier mode becomes unstable.

We have verified that, at the linear level, the dominant dynamic effect comes from the angular velocity Ω, and not from the angular acceleration $\dot{\Omega}$. Moreover, we have observed that the acceleration provokes only an overall rotation (phase modulation related to the imaginary part of the growth rate) of the interfacial patterns. This effect bears a curious resemblance to the phase drift that is so typical in the rotating Hele-Shaw cell dynamics with Coriolis effects [4,22–27].

The basic linear aspects discussed in Fig. 2 are obviously of interest, and useful to understand interface stability issues at the very beginning of the pattern formation process. But, unfortunately, one cannot assess the fundamentally important finger competition phenomena usually detected in rotating Hele-Shaw flows at the purely linear level. This key nonlinear facet of the problem, and the influence of $\Omega(t)$ and Re on its development, will be scrutinized in the next section, via a weakly nonlinear approach.

B. Nonlinear stage

From the weakly nonlinear, second-order perturbative studies performed in Refs. [16,41], it has been shown that the finger competition phenomena detected in Hele-Shaw cells can be accurately described by considering the coupling between the fundamental mode n and its subharmonic mode $n/2$. Therefore, to tackle finger competition issues at the weakly nonlinear level it is convenient to rewrite the net interface perturbation $\zeta(\theta,t)$ in terms of these two specific Fourier modes

$$\zeta(\theta,t) = \zeta_0 + a_n(t)\cos(n\theta) + b_n(t)\sin(n\theta) + a_{n/2}(t)\cos(n\theta/2) + b_{n/2}(t)\sin(n\theta/2), \quad (34)$$

where for a given mode $a_n(t) = [\zeta_n(t) + \zeta_{-n}(t)]$ and $b_n(t) = i[\zeta_n(t) - \zeta_{-n}(t)]$ denote the real-valued cosine and sine amplitudes, respectively. Besides, by imposing mass conservation (or, by keeping constant the area encircled by the two-fluid interface), we have that

$$\zeta_0 = -\frac{1}{4R}\{[a_n(t)]^2 + [a_{n/2}(t)]^2 + [b_n(t)]^2 + [b_{n/2}(t)]^2\}. \quad (35)$$

As demonstrated in Refs. [16,41], one can extract key information about the finger competition dynamics in Hele-Shaw flows by inspecting the behavior of the cosine and sine subharmonic perturbation amplitudes. The cosine perturbation amplitude $a_{n/2}$ breaks the n-fold rotational symmetry of the fundamental mode, by alternately increasing and decreasing the length of each of the n fingers. This effect describes competition of outward pointing fingers of the inner fluid. On the other hand, the sine perturbation amplitude $b_{n/2}$ distorts the fingers while varying the depths of the "valleys" between the outward pointing fingers. These valleys are in fact the inward pointing fingers of the outer fluid. It should be noted that, in rotating Hele-Shaw flows, both inward and outward pointing fingers are allowed to move in order to conserve mass in the fluid system.

This weakly nonlinear picture for finger competition (or finger length variability) in such a confined fluid flow environment is actually quite simple to grasp. For example, if one verifies that growth of $a_{n/2}$ is increased, while the growth of $b_{n/2}$ is inhibited, the result is an increased variability among the lengths of outward pointing fingers of the inner fluid. As pointed out above, this effect describes enhanced competition of the outward moving fingers. Note that this nonlinear competition mechanism determines the preferred direction for finger growth and finger length variability. In other words, if $a_{n/2}$ increases and $b_{n/2}$ decreases, even though there exists finger competition in both directions (outward and inward), the competition among outward pointing fingers is much stronger than the competition among inward pointing fingers. These conclusions are reversed if instead the growth of $b_{n/2}$ is favored over the growth of $a_{n/2}$. In this last case, competition of the inward pointing fingers of the outer fluid would have preferential growth.

It should be stressed that the validity and correctness of such a finger competition mechanism have been extensively tested by numerical simulations [18–21]. These sophisticated numerical studies have verified that the weakly nonlinear predictions regarding finger competition behavior [16,41]

remain valid for advanced time (fully nonlinear) stages of the rotating Hele-Shaw cell dynamics. As a matter of fact, the weakly nonlinear predictions are also in line with the rotating Hele-Shaw experiments conducted in Refs. [6,9,10].

The possibility of capturing important finger competition phenomena already at the lowest nonlinear level (i.e., at second-order in ζ) and by conveniently utilizing just two relevant Fourier modes (the fundamental n and its subharmonic $n/2$) should not be taken for granted. After all, the situation could have been much more complicated to describe via theoretical means. For instance, the inclusion of third, fourth, or higher perturbative orders could have been required, or the consideration of the coupling among many more Fourier modes could have been necessary. These observations justify the usefulness of our analytical weakly nonlinear calculations for rotating Hele-Shaw flows in which the effects of $\Omega(t)$ and Re are taken into account. Regarding other alternative approaches, for instance, the solution and description of the system through intensive, fully nonlinear numerical simulations, it is not exactly trivial to implement, and is indeed much more expensive computationally. Therefore, to probe the onset of nonlinear effects (e.g., finger competition events) in our confined rotating flow system, the weakly nonlinear scheme we employ in this work stands as a valuable theoretical tool.

To examine the finger competition behavior under time-dependent angular velocity and nonvanishing Re conditions, one needs to describe the time evolution of the interface by using Eqs. (34) and (35). Specifically, one has to know how the amplitudes $a_n(t)$, $b_n(t)$, $a_{n/2}(t)$, and $b_{n/2}(t)$ evolve in time. In practical terms, we do this by rewriting the complex amplitude representation of the mode-coupling equation (20) in terms of the real-valued sine and cosine modes, by considering the interplay of modes n and $n/2$, and then numerically solving the resulting coupled nonlinear differential equations. Following Refs. [16,41], without loss of generality, we choose the phase of the fundamental mode so that $a_n(t) > 0$ and $b_n(t) = 0$. Another way to obtain the nonlinear evolution of the rotating interface is through the combination of the linear solution (29) with the nonlinear equation (20). Since in this work we are considering terms up to second order in ζ, we can replace $\zeta_{n'}$ and $\zeta_{n-n'}$ (and their derivatives) in the nonlinear terms on the right-hand side of Eq. (20) by the exact linear solution (29). This calculation results in a very complicated ordinary differential equation for ζ_n that represents the early stages of the nonlinear dynamics. Finally, one can rewrite this resulting differential equation to obtain coupled differential equations for the modes $a_n(t)$, $b_n(t)$, $a_{n/2}(t)$, and $b_{n/2}(t)$, and only after this solve them numerically.

Before proceeding to the analysis of the finger competition responses under time-dependent angular velocity and $\mathrm{Re} \neq 0$ circumstances, we briefly comment on what is already well known regarding the finger competition dynamics in rotating Hele-Shaw flows with constant angular velocity and $\mathrm{Re} = 0$. It has been reported that, under constant angular velocity and negligible Re, finger competition depends strongly on the viscosity ratio $\beta = \eta_2/\eta_1$ [6,9,10,16,18–21]. Namely, if $0 \leqslant \beta < 1$ ($\beta > 1$) one finds enhanced competition among inward (outward) pointing fingers. Moreover, it has also been verified that finger competition (for both inward and outward pointing fingers) is significantly inhibited when $\beta = 1$. In this section, we investigate how these conventional (constant angular velocity, and vanishing Re) finger competition reactions to changes in the viscosity ratio are affected, if the angular velocity of the rotating Hele-Shaw cell varies in time, and if inertial effects are taken into consideration.

To study the weakly nonlinear finger competition behaviors expressed by typical pattern-forming structures in a rotating Hele-Shaw with the time-dependent angular velocity given by Eq. (28), we begin our discussion by examining Fig. 3. In this figure, we set $\gamma = 2$, and consider three increasing values of the Reynolds number: (a) $\mathrm{Re} = 0.03$, (b) $\mathrm{Re} = 0.16$, and (c) $\mathrm{Re} = 0.2$. On the top panels, we plot the time evolution of the fluid-fluid interfaces considering the interaction of the fundamental mode $n = 10$, and its subharmonic $n/2 = 5$. The time varies in the range $0 \leqslant t \leqslant t_f$, where the final time t_f is defined as the time at which the amplitude of the fundamental mode has reached the same magnitude [namely, $a_n(t = t_f) = 0.15$] for each value assumed by Re. This is done with no loss of generality, in order to make the generated patterns to have approximately the same size at $t = t_f$. The various interfaces are plotted separated by equally spaced time steps $\Delta t = t_f/25$. On the

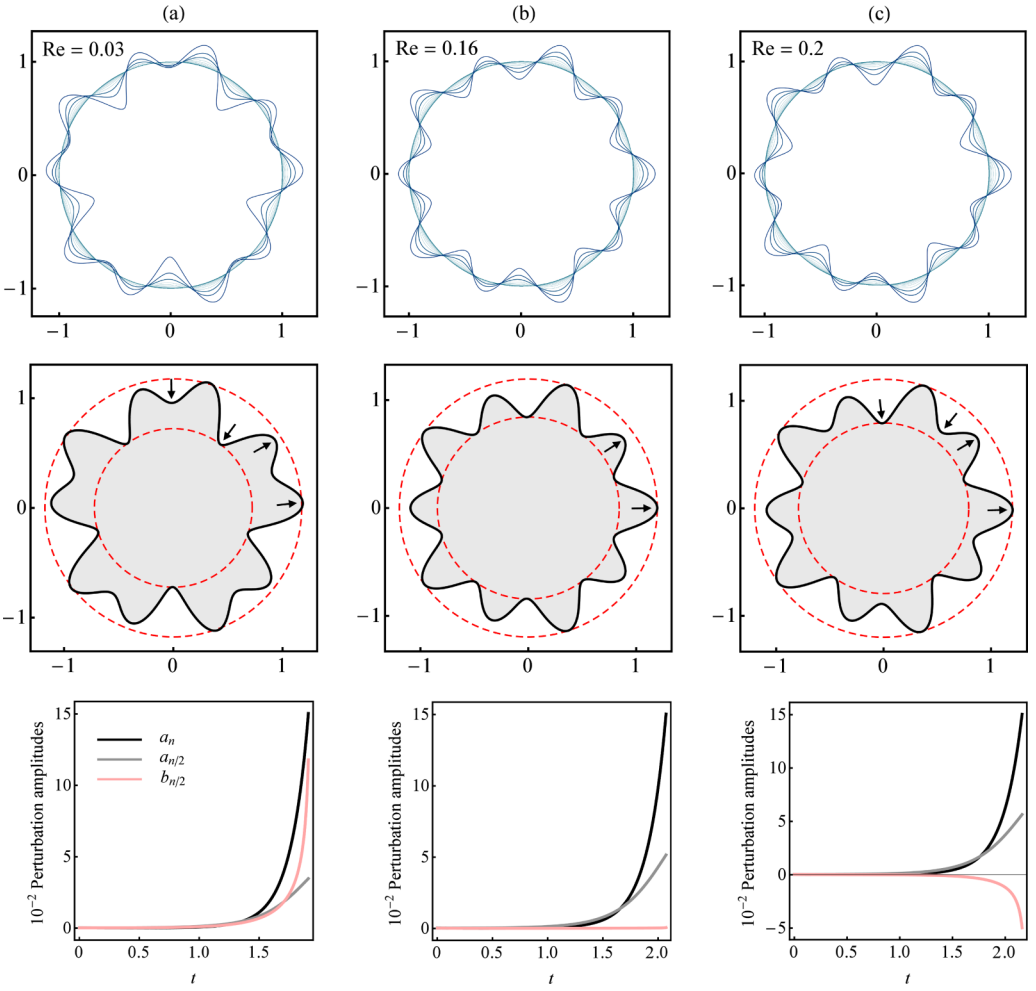

FIG. 3. Time overlaid plots (top panels) illustrating the typical evolution of the two-fluid interfaces obtained in rotating Hele-Shaw flows, for a time-dependent angular velocity given by Eq. (28) with $\gamma = 2$ and three increasing values of the Reynolds number: (a) Re $= 0.03$, (b) Re $= 0.16$, and (c) Re $= 0.2$. The resulting fingering patterns (shaded areas) obtained at the final time $t = t_f$ are shown in the middle panels. The snapshots are taken for times (a) $t_f = 1.9107$, (b) $t_f = 2.072$, and (c) $t_f = 2.1599$, where t_f is defined as the time at which the amplitude of the fundamental mode has reached the value $a_n(t = t_f) = 0.15$, for each value of Re. The small arrows point in the direction of inward or outward motion of the competing fingers. The dashed circles are added to facilitate visualization of the competition among the fingers. The corresponding time evolution of the perturbation amplitudes $a_n(t)$, $a_{n/2}(t)$, and $b_{n/2}(t)$, for modes $n = 10$ and $n/2 = 5$ is depicted in the bottom panels. We set $\alpha = 10^{-3}$, $\beta = 0$, and $B = 3.0 \times 10^{-3}$.

middle panels, we depict snapshots of the resulting interfacial patterns produced at final times $t = t_f$. For clarity, the final shapes have been shaded. The small arrows indicate the direction of motion (inward, or outward) of the competing fingers, and the dashed circles guide the eye, helping in the visualization of finger competition events. Finally, on the bottom panels, we show the corresponding time evolution of the perturbations amplitudes a_n, $a_{n/2}$, and $b_{n/2}$. In Fig. 3, similarly to what we did in Fig. 2, we consider a situation widely explored experimentally, in which the inner fluid is much more dense and viscous than the outer fluid. Under such circumstances we choose $\alpha = 10^{-3}$, $\beta = 0$,

and $B = 3.0 \times 10^{-3}$. In addition, we take the initial conditions $a_n(0) = 3.3 \times 10^{-4}$, and $a_{n/2}(0) = b_{n/2}(0) = 2.5 \times 10^{-4}$. Likewise, we pick $\dot{a}_n(0) = -9.9 \times 10^{-4}$ and $\dot{a}_{n/2}(0) = \dot{b}_{n/2}(0) = 0$.

We call the reader's attention to a very important point about the way data are presented in Fig. 3. It is worth noting that, for the values of time chosen to display the interfacial patterns depicted in Figs. 3(a)–3(c), the angular velocities have almost reached a steady value, in the sense that they are all approximately equal to Ω_0 ($\approx 0.98\Omega_0$). Therefore, for these times, the transient regime in which the system effectively accelerates is basically over. In this way, in Fig. 3 we compare different situations (each having a different Re), but all of them are considered at times in which the instantaneous angular velocities are all very similar to one another.

We initiate our discussion by surveying Fig. 3(a), which considers a very small Reynolds number situation (Re = 0.03). From the interface time evolution depicted in the top panel, and with the guidance of the auxiliary dashed circles and small arrows indicated in the middle panel of Fig. 3(a), one readily verifies a strong competition among the inward pointing fingers of the outer fluid, as well as a not so intense competition among the outward pointing fingers of the inner fluid. These visual findings are in agreement with what is shown more quantitatively in the bottom panel of Fig. 3(a), where we see an enhanced growth of the sine subharmonic $b_{n/2}(t)$, as opposed to a comparatively modest growth of the cosine subharmonic $a_{n/2}(t)$. All this information is not entirely surprising, since it is well established (for the usual constant angular velocity situation, and very small Re) [6,9,10,16,18–21] that for $\beta = 0$ the most prominent finger competition feature is indeed a strong competition among inward pointing fingers. Therefore, even though in Fig. 3(a) the angular velocity is actually varying in time, since the Reynolds number is so small, the finger competition behavior for $\gamma = 2$ is not that different from the one typically found under constant angular velocity conditions ($\gamma \to \infty$).

A significantly different scenario is revealed in Fig. 3(b), where a larger Reynolds number is used (Re = 0.16). Now, from the top and middle panels of Fig. 3(b) it is apparent that, in contrast to what is observed in Fig. 3(a), there is no competition among the inward pointing fingers. In addition, one also notices an increased competition among the outward pointing fingers. These pictorial conclusions are supported by the complementary results presented on the bottom panel of Fig. 3(b), where $b_{n/2}(t)$ is nearly zero and does not change as time progresses. On the other hand, one can see that $a_{n/2}(t)$ grows at later times, reaching a final magnitude that is a bit larger than the one obtained in Fig. 3(a). From these observations, and knowing that here $\beta = 0$, we can say that these results for Re = 0.16 are certainly unexpected. A comparative analysis between Fig. 3(a) and Fig. 3(b) does indicate that, depending on the value of Re, the finger competition responses obtained under a time-varying angular velocity situation can be considerably different.

In Fig. 3(c) we analyze a situation in which an even higher value of the Reynolds number is utilized (Re = 0.2). By examining the top and middle panels of Fig. 3(c), we find noticeable competition among both inward and outward pointing fingers. The resulting finger competition behavior in Fig. 3(c) is a sort of combination of part of the finger competition responses already observed in Fig. 3(a), and in Fig. 3(b). More specifically, in Fig. 3(c) the inward pointing fingers behave similarly to the inward pointing fingers of Fig. 3(a), while the outward moving fingers of Fig. 3(c) react as the outward moving fingers of Fig. 3(b). These remarks can be better understood by going through the data depicted in the bottom panel of Fig. 3(c). By increasing Re further away from its value at which $b_{n/2}(t) = 0$ [namely, Re = 0.16 as in Fig. 3(b)], the result is inducing the growth of a negative sine perturbation amplitude. So, as in Fig. 3(a), the magnitude of $b_{n/2}(t)$ in Fig. 3(c) increases as time advances, but in the end it reaches a smaller value. However, instead of being positive, $b_{n/2}(t)$ acquires negative values. It turns out that this change in sign is inconsequential with respect to the dominant finger competition behavior for the inward pointing fingers. Additionally, considering that the growth of $a_n(t)$, and $a_{n/2}(t)$ are quite similar in Figs. 3(b) and in 3(c), it is no surprise to find similar behaviors for the outward pointing fingers in these two situations.

From Fig. 3 it is evident that the major effects related to changes in Re under time-dependent angular velocity circumstances are reflected on the growth of the sine perturbation amplitude $b_{n/2}(t)$, which is significant in Fig. 3 (a), nearly zero in Fig. 3(b), and again sizable in Fig. 3(c). Consequently,

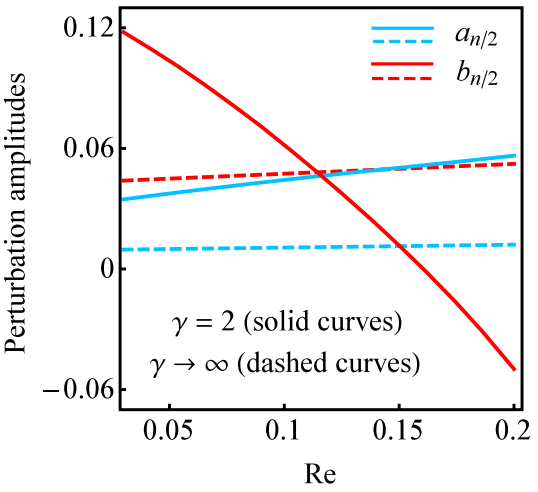

FIG. 4. Behavior of the perturbation amplitudes $a_{n/2}$ and $b_{n/2}$ as the Reynolds number Re is changed under constant angular velocity ($\gamma \to \infty$, represented by the dashed curves), and under a time-dependent angular velocity condition ($\gamma = 2$, symbolized by the solid curves). All physical parameters and initial conditions are the same as the ones used in Fig. 3.

one may say that the consideration of a time-varying angular velocity and inertial effects allows a welcome flexibility for the possible finger competition outcomes when $\beta = 0$. If $\beta = 0$, and the angular velocity is constant, one always finds the same dominant dynamic response: i.e., a stronger competition among inward pointing fingers. Conversely, if $\beta = 0$, and the angular velocity varies in time, one can make this competition behavior among inward fingers to decrease, to simply disappear, or yet to increase again, just by properly adjusting the value of the Reynolds number.

As a final remark about the results extracted from Fig. 3, one should realize that the reason behind the fact that the finger competition behavior illustrated in Fig. 3(a) for $\Omega = \Omega(t)$ to be almost identical to the one that occurs at constant angular velocity, is not due to the particular exponentially increasing form of Eq. (28) (for which a transient regime naturally arises). But it is related to the fact that the Reynolds number used in Fig. 3(a) is very low (Re $= 0.03$). This is exactly what happened in Ref. [7]: despite dealing with a time-dependent angular velocity [also given by Eq. (28)], their experimental findings (obtained at very low Re) showed no difference to those obtained at the regime in which the angular velocity is constant in time. The key role played by Re becomes evident by examining Fig. 3(b), which utilizes the very same $\Omega(t)$ used in Fig. 3(a) but detects a finger competition response that is quite distinct from the one observed at a constant angular velocity condition. This is verified because in Fig. 3(b) a significantly larger Reynolds number is used (Re $= 0.16$). Actually, this last remark is also applied to Fig. 3(c). Moreover, this happens irrespective of the fact that a transient is still present in Fig. 3(b) and in Fig. 3(c). So the results presented in Fig. 3 show that the effects of a time-dependent angular velocity are consequential for the finger competition dynamics, only if one considers sufficiently large Reynolds numbers. Is is also worth noting that the weakly nonlinear theory we developed is valid to a general form, time-dependent angular velocity $\Omega(t)$, and not at all restricted to the particular exponential form given in Eq. (28). In fact, Eqs. (20)–(26) apply to a much more general situation that may involve, or not, the existence of an eventual transient regime.

Supplementary information about the changes occurring in the finger competition behavior when the Reynolds number is varied is provided by Fig. 4. By using the very same set of physical parameters, and initial conditions utilized in Fig. 3, Fig. 4 illustrates how the perturbation amplitudes $a_{n/2}$ and $b_{n/2}$ behave as the Reynolds number continuously sweeps the range of values $0 \leqslant \text{Re} \leqslant 0.2$. This is done for a constant angular velocity situation ($\gamma \to \infty$, portrayed by the dashed curves), as well as for a time-dependent angular velocity condition ($\gamma = 2$, represented by the solid curves).

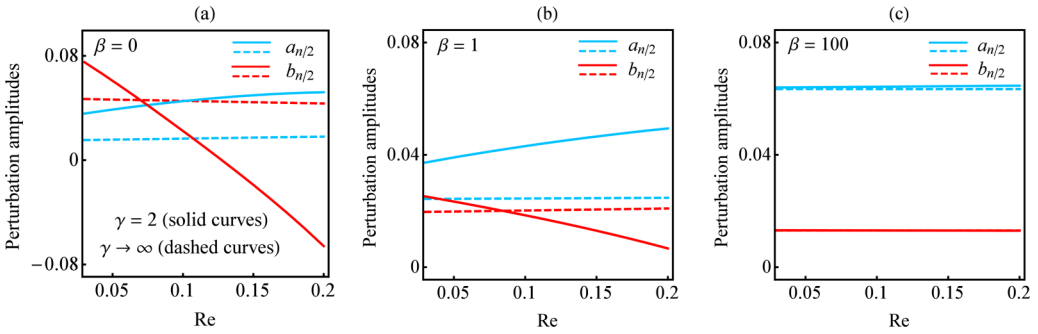

FIG. 5. Variation of the perturbation amplitudes $a_{n/2}$ and $b_{n/2}$ as the Reynolds number Re is varied, under constant angular velocity ($\gamma \to \infty$, expressed by the dashed curves), and under a time-dependent angular velocity condition ($\gamma = 2$, pictured by the solid curves). Three representative values for the viscosity ratio are considered: (a) $\beta = 0$, (b) $\beta = 1$, and (c) $\beta = 100$. Here we take $\alpha = 0.5$, $n = 8$, and $n/2 = 4$. All other physical parameters and initial conditions are exactly the same as the ones employed in Fig. 3.

Similarly to what has been done in Fig. 3, the times for which Fig. 4 is plotted are the times at which the perturbation amplitude of the fundamental mode has reached the magnitude $a_n = 0.15$, for each value assumed by the Reynolds number. This criterion for setting the times used in the plots is also applied to Fig. 5. By observing the dashed curves in Fig. 4, it is apparent that the magnitudes of $a_{n/2}$ and $b_{n/2}$ do not change much if the angular velocity is constant. This means that, within the low Reynolds number situation considered here ($\mathrm{Re}^2 \ll 1$), the finger competition behavior is almost insensitive to changes in Re, if the angular velocity of the rotating Hele-Shaw cell is constant in time. Nevertheless, a completely different scheme is unveiled when we follow the changes experienced by the solid curves when Re is modified. Although the changes in the cosine subharmonic amplitude $a_{n/2}$ are not really impressive as Re is increased, the corresponding modifications in the sine subharmonic amplitude $b_{n/2}$ are much more intense. As Re is increased, the magnitude of $b_{n/2}$ drops significantly, ultimately reaching a zero value. As a consequence, the competition among inward pointing is decreased and eventually ceases during this process. So, in spite of the fact that $\beta = 0$, by increasing Re, there is a clear tendency to decrease the competition among inward fingers, accompanied by a simultaneous inclination to moderately increase competition among outward pointing fingers. Nonetheless, as Re is increased further, the sign of $b_{n/2}$ becomes negative, but its magnitude starts to increase again. In this case, the result is the reoccurrence of finger competition among inward and outward pointing fingers. The findings of Fig. 4 for a range of values of Re generalize and substantiate the results discussed in Fig. 3 for just three particular values of Re. Therefore, on the basis of these facts, one can see that, for $\beta = 0$, the finger competition scenario for a time-dependent angular velocity $\Omega(t)$ and $\mathrm{Re} \neq 0$ is considerably richer than the one associated to the simpler constant angular velocity situation at $\mathrm{Re} = 0$.

As mentioned earlier in this work, it is well known that, under the condition of constant angular velocity, the finger competition behavior in rotating Hele-Shaw cells depends strongly on the viscosity ratio β [6,9,10,16,18–21]. Therefore, it is of interest to revisit the situations examined in Figs. 3 and 4, which are restricted to the case $\beta = 0$, and explore them further by considering other values of the viscosity ratio. This is done in Fig. 5, which illustrates how the perturbation amplitudes $a_{n/2}$ and $b_{n/2}$ respond to changes in the Reynolds number Re, considering both constant (dashed curves) and time-varying (solid curves) angular velocities, for three characteristic values of the viscosity ratio: (a) $\beta = 0$, (b) $\beta = 1$, and (c) $\beta = 100$. In order to assess such values of β, and still keep a close connection to the typical material properties of the fluids involved in real experiments, here we consider that the density ratio is $\alpha = 0.5$. In addition, we take $n = 8$, and $n/2 = 4$. However, the remaining physical parameters, and all initial conditions are identical to those utilized in Fig. 4.

First, in Fig. 5(a) we consider the situation in which $\beta = 0$ (outer fluid is inviscid). Despite the fact that in Fig. 5(a) $\beta = 0$, and $\alpha = 0.5$, while in Fig. 4 $\beta = 0$, and $\alpha = 10^{-3}$, the way the amplitudes

$a_{n/2}$ and $b_{n/2}$ react to changes in Re is rather similar in both cases. If the angular velocity is kept constant (dashed curves), the amplitudes $a_{n/2}$ and $b_{n/2}$ hardly change as Re is increased, meaning that the finger competition events are basically indifferent to variations in the Reynolds number under such conditions. Nevertheless, if the angular velocity is time-dependent (solid curves), one easily identifies that $b_{n/2}$ changes significantly as Re is augmented ($b_{n/2}$ decreases consistently to zero, and then changes in sign), while $a_{n/2}$ just increases modestly. So, as it happened in Fig. 4, as Re grows in Fig. 5(a) one should expect an initial decrease in the competition of inward fingers, followed by a situation in which such competition goes to zero and then reappears. Likewise, all this happens while the competition among outward pointing fingers (measured by $a_{n/2}$) mildly increases as Re assumes larger values.

Now we turn to Fig. 5(b) which focuses on the viscosity-matched situation $\beta = 1$. If the angular velocity is constant (dashed curves), we see that the amplitudes $a_{n/2}$ and $b_{n/2}$ remain quite small, and nearly unchanged as Re is varied. So, as expected for the situation in which $\beta = 1$ and $\gamma \to \infty$, the competition among inward as well as among outward fingers is tempered. This finger competition dynamical response changes considerably if the angular velocity is time-dependent (solid curves). If $\gamma = 2$, one finds that the cosine (sine) perturbation amplitude increases (decreases) if the Reynolds number is increased. As a result, although $\beta = 1$, since the angular velocity varies in time, one encounters enhanced (restrained) competition among outward (inward) fingers as Re reaches higher magnitudes.

Last, we investigate Fig. 5(c) which takes a higher value of the viscosity ratio ($\beta = 100$), meaning that the outer fluid is significantly more viscous than the inner fluid. Recall that for a constant angular velocity, we anticipate the occurrence of an increased competition among outward pointing fingers. This is precisely what we find in Fig. 5(c), as expressed by the dashed curves, where the magnitude of $a_{n/2}$ is considerably greater than the magnitude of $b_{n/2}$. As usual, for this $\gamma \to \infty$ case, these responses do not change much if Re is modified. Amazingly enough, the same type of finger competition behavior is observed if the angular velocity varies in time. As a matter of fact, as readily identified in Fig. 5(c), if $\beta = 100$ the finger competition behavior for constant and time-dependent angular velocities are almost indistinguishable. From Figs. 5(a)–5(c), one realizes that the impact of the time-dependent angular velocity and inertia on the finger competition mechanism becomes increasingly less important as the viscosity ratio is enlarged. So, regarding the sensitivity of finger length variability when a whole range of allowed magnitudes for β is considered, we have verified that the most significant effects related to the action of $\Omega(t)$ and Re should arise at relatively low values of β (i.e., $0 \leqslant \beta \leqslant 10$).

IV. CONCLUSION

We have studied some aspects of the dynamics in a rotating Hele-Shaw cell which spins with a time-dependent angular velocity $\Omega(t)$. Proper evaluation of the effects caused by $\Omega(t)$ on the fluid-fluid interface behavior requires the inclusion of inertial effects. Hence, we tackled the interfacial pattern formation problem in such a confined rotating fluid flow environment, by utilizing a generalized Darcy's law approach. This allowed us to take into consideration the impact of the Reynolds number Re and $\Omega(t)$ on the linear stability, as well as on nonlinear finger competition dynamics of the system.

By employing a perturbative mode-coupling theory, and considering low values of Re ($\mathrm{Re}^2 \ll 1$), we have derived an equation of motion for the two-fluid interface. Such a nonlinear differential equation describes the time evolution of the perturbation amplitudes up to second-order [$\mathrm{O}(\zeta^2)$] accuracy, for arbitrary viscosity and density ratios.

At the linear level [$\mathrm{O}(\zeta)$], we detected the development of a peculiar cascade of modes which become increasingly unstable with time due to the action of $\Omega(t)$. In addition, we have found that inertial effects tend to stabilize the system, by decreasing the magnitude of the growth rate, and by introducing delay effects into the linear stability dynamics. However, the most significant findings

regarding the influence of $\Omega(t)$ and Re on the two-fluid interface have been unveiled at the weakly nonlinear regime.

At the onset of nonlinearities [$O(\zeta^2)$], we have found that the interplay of $\Omega(t)$ and Re significantly affects the finger competition events, inducing the emergence of various changes in the traditional (constant angular velocity) finger length variability behavior of the system, as the density and the viscosity ratios are changed.

In conclusion, our linear and weakly nonlinear results indicate that the time-dependent angular velocity $\Omega(t)$ and inertia ($\mathrm{Re} \neq 0$) introduce a number of nontrivial modifications into the conventional rotating Hele-Shaw problem (for which Ω is constant in time, and $\mathrm{Re} = 0$). Based on the possibilities opened up by our theoretical predictions, we hope our findings will motivate researchers to try to check them experimentally in the future, considering non-negligible Reynolds number conditions.

ACKNOWLEDGMENTS

J.A.M. thanks CNPq (Brazilian Research Council) for financial support under Grant No. 304821/2015-2. E.O.D. acknowledges financial support from FACEPE through PPP Project No. APQ-0800-1.05/14. We are indebted to Rodolfo Brandão for useful discussions and for assisting us to find a closed-form solution for Eq. (27).

[1] P. G. Saffman and G. I. Taylor, The penetration of a fluid into a porous medium or Hele-Shaw cell containing a more viscous liquid, Proc. R. Soc. London Ser. A **245**, 312 (1958).

[2] L. Paterson, Radial fingering in a Hele-Shaw cell, J. Fluid Mech. **113**, 513 (1981).

[3] G. M. Homsy, Viscous fingering in porous media, Annu. Rev. Fluid Mech. **19**, 271 (1987); K. V. McCloud and J. V. Maher, Experimental perturbations to Saffman-Taylor flow, Phys. Rep. **260**, 139 (1995); J. Casademunt, Viscous fingering as a paradigm of interfacial pattern formation: Recent results and new challenges, Chaos **14**, 809 (2004).

[4] L. W. Schwartz, Instability and fingering in a rotating Hele-Shaw cell or porous medium, Phys. Fluids A **1**, 167 (1989).

[5] J. Casademunt, Exploring topological singularities with phase-field methods. Centrifugal viscous fingering as a case study, Eur. Phys. J. Plus **126**, 94 (2011), and references therein.

[6] Ll. Carrillo, F. X. Magdaleno, J. Casademunt, and J. Ortín, Experiments in a rotating Hele-Shaw cell, Phys. Rev. E **54**, 6260 (1996).

[7] Ll. Carrillo, J. Soriano, and J. Ortín, Radial displacement of a fluid annulus in a rotating Hele-Shaw cell, Phys. Fluids **11**, 778 (1999).

[8] Ll. Carrillo, J. Soriano, and J. Ortín, Interfacial instabilities of a fluid annulus in a rotating Hele-Shaw cell, Phys. Fluids **12**, 1685 (2000).

[9] E. Alvarez-Lacalle, J. Ortín, and J. Casademunt, Low viscosity contrast fingering in a rotating Hele-Shaw cell, Phys. Fluids **16**, 908 (2004).

[10] E. Alvarez-Lacalle, J. Ortín, and J. Casademunt, Relevance of dynamic wetting in viscous fingering patterns, Phys. Rev. E **74**, 025302(R) (2006).

[11] V. M. Entov, P. I. Etingof, and D. Ya. Kleinbock, On nonlinear interface dynamics in Hele-Shaw flows, Eur. J. Appl. Math. **6**, 399 (1995).

[12] F. X. Magdaleno, A. Rocco, and J. Casademunt, Interface dynamics in Hele-Shaw flows with centrifugal forces: Preventing cusp singularities with rotation, Phys. Rev. E **62**, R5887 (2000).

[13] D. Crowdy, Theory of exact solutions for the evolution of a fluid annulus in a rotating Hele-Shaw cell, Q. Appl. Math. **60**, 11 (2002).

[14] N. R. McDonald, Generalised Hele-Shaw flow: A Schwarz function approach, Eur. J. Appl. Math. **22**, 517 (2011).

[15] M. Ehrnström, J. Escher, and B. V. Matioc, Well-posedness, instabilities, and bifurcation results for the flow in a rotating Hele-Shaw cell, J. Math. Fluid Mech. **13**, 271 (2011).

[16] H. Gadêlha and J. A. Miranda, Finger competition dynamics in rotating Hele-Shaw cells, Phys. Rev. E **70**, 066308 (2004).
[17] C.-Y. Chen and S.-W. Wang, Interfacial instabilities of miscible fluids in a rotating Hele-Shaw cell, Fluid Dyn. Res. **30**, 315 (2002).
[18] C.-Y. Chen, C.-H. Chen, and J. A. Miranda, Numerical study of pattern formation in miscible rotating Hele-Shaw flows, Phys. Rev. E **73**, 046306 (2006).
[19] J. A. Miranda and E. Alvarez-Lacalle, Viscosity contrast effects on fingering formation in rotating Hele-Shaw flows, Phys. Rev. E **72**, 026306 (2005).
[20] R. Folch, E. Alvarez-Lacalle, J. Ortín, and J. Casademunt, Pattern formation and interface pinch-off in rotating Hele-Shaw flows: A phase-field approach, Phys. Rev. E **80**, 056305 (2009).
[21] C.-Y. Chen, Y.-S. Huang, and J. A. Miranda, Diffuse-interface approach to rotating Hele-Shaw flows, Phys. Rev. E **84**, 046302 (2011).
[22] S. L. Waters and L. J. Cummings, Coriolis effects in a rotating Hele-Shaw cell, Phys. Fluids **17**, 048101 (2005).
[23] S. L. Waters, L. J. Cummings, K. M. Shakesheff, and F. R. A. J. Rose, Tissue growth in a rotating bioreactor. Part I: Mechanical stability, IMA J. Math. Appl. Med. Biol. **23**, 311 (2006).
[24] A. Abidate, S. Aniss, O. Caballina, and M. Souhar, Effects of circular rigid boundaries and Coriolis forces on the interfacial instability in a rotating annular Hele-Shaw cell, Phys. Rev. E **75**, 046307 (2007).
[25] E. Alvarez-Lacalle, H. Gadêlha, and J. A. Miranda, Coriolis effects on fingering patterns under rotation, Phys. Rev. E **78**, 026305 (2008).
[26] C.-Y. Chen, C.-W. Huang, H. Gadêlha, and J. A. Miranda, Radial viscous fingering in miscible Hele-Shaw flows: A numerical study, Phys. Rev. E **78**, 016306 (2008).
[27] J. A. Miranda, H. Gadêlha, and A. T. Dorsey, Coriolis effects on rotating Hele-Shaw flows: A conformal mapping approach, Phys. Rev. E **82**, 066306 (2010).
[28] J. Bouchgl, S. Aniss, M. Souhar, and A. Hifdi, Interfacial instability in a time-periodic rotating Hele-Shaw cell, MATEC Web conferences **16**, 09004 (2014).
[29] P. Gondret and M. Rabaud, Shear instability of two-fluid parallel flow in a Hele-Shaw cell, Phys. Fluids **9**, 3267 (1997).
[30] C. Ruyer-Quil, Inertial corrections to the Darcy law in a Hele-Shaw cell, C. R. Acad. Sci. Ser. IIb: Mec. **329**, 337 (2001).
[31] F. Plouraboue and E. J. Hinch, Kelvin-Helmholtz instability in a Hele-Shaw cell, Phys. Fluids **14**, 922 (2002).
[32] C. Chevalier, M. Ben Amar, D. Bonn, and A. Lindner, Inertial effects on Saffman-Taylor viscous fingering, J. Fluid Mech. **552**, 83 (2006).
[33] A. He and A. Belmonte, Inertial effects on viscous fingering in the complex plane, J. Fluid Mech. **668**, 436 (2011).
[34] E. O. Dias and J. A. Miranda, Inertial effects on rotating Hele-Shaw flows, Phys. Rev. E **83**, 046311 (2011).
[35] E. O. Dias and J. A. Miranda, Influence of inertia on viscous fingering patterns: Rectangular and radial flows, Phys. Rev. E **83**, 066312 (2011).
[36] C.-W. Park and G. M. Homsy, Two-phase displacement in Hele-Shaw cells: Theory, J. Fluid Mech. **139**, 291 (1984).
[37] S. J. Jackson, D. Stevens, D. Giddings, and H. Power, Dynamic-wetting effects in finite-mobility-ratio Hele-Shaw flow, Phys. Rev. E **92**, 023021 (2015).
[38] P. H. A. Anjos and J. A. Miranda, Radial viscous fingering: Wetting film effects on pattern-forming mechanisms, Phys. Rev. E **88**, 053003 (2013).
[39] P. H. A. Anjos and J. A. Miranda, Influence of wetting on fingering patterns in lifting Hele-Shaw flows, Soft Matter **10**, 7459 (2014).
[40] S. S. S. Cardoso and A. W. Woods, The formation of drops through viscous instability, J. Fluid Mech. **289**, 351 (1995).
[41] J. A. Miranda and M. Widom, Radial fingering in a Hele-Shaw cell: A weakly nonlinear analysis, Physica D **120**, 315 (1998).